Ceramics International 51 (2025) 16629–16639

Contents lists available at ScienceDirect

Ceramics International

journal homepage: www.elsevier.com/locate/ceramint

$YPO_4:Yb^{3+}$ and $Al_2O_3:Cr^{3+}$ containing fibers with optical on/off gain using glass powder doping

Dominik Dorosz [a,*], Marcin Kochanowicz [b], Rafael Valiente [c], Robert Müller [d], Andrea Diego-Rucabado [c], Fernando Rodríguez [c], Nuria Siñeriz-Niembro [c], José I. Espeso [c], Magdalena Lesniak [a], Piotr Miluski [b], Sylvia Conzendorf [e], Juliane Posseckardt [e], Zhongquan Liao [e], Gloria Lesly Jimenez [a], Martin Lorenz [d], Anka Schwuchow [d], Martin Leich [d], Adrian Lorenz [d], Katrin Wondraczek [d], Matthias Jäger [d]

[a] AGH University of Krakow, A. Mickiewicza Av. 30, 30-059, Kraków, Poland
[b] Bialystok University of Technology, Wiejska 45D Street, 15-351, Bialystok, Poland
[c] University of Cantabria, Avenida. de Los Castros 48., 39005, Santander, Spain
[d] Leibniz Institute of Photonic Technology, Albert-Einstein-Str. 9, 07745, Jena, Germany
[e] Fraunhofer Institute for Ceramic Technologies and Systems IKTS, Maria-Reiche-Str. 2, 01109, Dresden, Germany

ARTICLE INFO

Handling Editor: Dr P. Vincenzini

Keywords:
Optical fibers
Glass ceramics
Glass powder-NCs doping method
$YPO_4:Yb^{3+}$ nanocrystals

ABSTRACT

The glass-powder-nanocrystals (NCs) method was investigated as a powerful technique to develop new optical fibers in the context of fiber lasers and amplifiers applications. The advantage of this method is the independent preparation of NCs and matrix glass, which gives full control of the crystal phase and active ion concentration of the NCs as well as the refractive index of the glass, resulting in index matching. We demonstrated the survival of $YPO_4:Yb^{3+}$ and $Al_2O_3:Cr^{3+}$ NCs in defect-free short optical fibers, pointing out essential key issues like optimization of the NCs content in the core and their mixing procedure as well as densification (pressing and pre-sintering) of the core material and effective route to lower scattering losses using smaller NCs size (150 nm). The importance of avoiding secondary crystallization has been discussed in the example of embedding two different NCs in the commercial Ohara glass matrix. In developed $YPO_4:Yb^{3+}$ doped optical fiber, we achieved a relatively large on/off gain coefficient of about 1 dB/cm. This result makes glass-powder-doped fibers interesting for fiber sensors and promising for fiber lasers and amplifier applications after further optical quality improvement.

1. Introduction

Optical materials doped with rare-earth ions (REs) play an important role in many photonic devices, especially lanthanide-doped crystals and optical fibers for lasers and light sources. The specific lasing features inherent to the kind of host, like narrow emission lines in crystals and large laser interaction lengths in optical fibers, can be combined in optical glass-crystalline fiber (G-CF), where RE-doped nanocrystals (NCs) are embedded in the core volume. Even though such fiber architecture seems highly interesting, the complex topic of hybrid glass-crystalline NCs for laser applications is slowly entering current research.

In the last decades, research has been dedicated to the study of three approaches: (a) direct NC incorporation, (b) in-process formation of NCs during fiber drawing, and (c) thermal G-CF post-treatment to obtain laser active nanocrystals in fibers. Samson et al. obtained the most impressive results for the post-treatment of fibers more than 20 years ago [1]. Unfortunately, the thermal treatment of drawn fibers typically destroys the coating material required for the fiber's mechanical strength. A successful G-CF post-treatment approach yielded $NaLuF_4:Yb^{3+}/Er^{3+}$ NCs, exhibiting a blue transition and a significant increase in green and red upconversion emission [2]. Another approach, i.e., direct NCs doping, was achieved by direct NCs incorporation into glass [3,4] or fiber preforms [5,6] and optical fibers doped with $LiYF_4:Yb^{3+}/Er^{3+}$, achieving 50 % NCs survival with a loss of ~0.5 dB/m at @1300 nm [3], phosphate fiber doped with $SrAl_2O_4:Eu^{2+}/Dy^{3+}$ crystalline phosphors [4]; $YbPO_4$ crystals containing fibers via MCVD-solution doping [5], and

* Corresponding author.
E-mail address: ddorosz@agh.edu.pl (D. Dorosz).

https://doi.org/10.1016/j.ceramint.2025.01.277
Received 21 October 2024; Received in revised form 10 January 2025; Accepted 14 January 2025
Available online 15 January 2025

powder-in-tube derived fibers [6]. The in-process NCs formation during fiber drawing can successfully generate NCs in fiber. It strongly relies on designing a preform core composition in which, according to phase diagrams, crystallization is expected to occur within the thermal conditions during fiber fabrication: YAG crystals in a preform dissolved upon heat treatment, obtaining YPO_4 NCs with different morphologies depending on the drawing temperature [7]. In antimony-silicate glass, YPO_4:Eu^{3+} crystals could be obtained during drawing [8].

When analyzing recent reports on glass-crystalline optical fibers, one needs to distinguish optical properties resulting from crystalline and amorphous phases. High laser action and the optical net gain is only accessible via low scattering, and thus low attenuation values, which in turn can only be realized if the criteria of NCs size is met, i.e., sufficiently small NCs depending on their refractive index relative to that of the host matrix [9]. Another aspect of all G-CF is the co-existence of active dopants in both the crystalline phase and the glassy matrix. This might result from incomplete crystallization during thermal treatment and partial crystal dissolution effects in the case of crystal doping. To reduce the crystalline fraction in the amorphous phase and to confine the crystals, one possibility is to enforce crystallization by adding a nucleating agent such as lanthanide ions, for example, crystalline SnO_2:Er^{3+} in planar waveguides [10]. On the other hand, the dissolution effect observed in NCs directly mixed with the surrounding glass has been attributed to complex thermal and chemical interactions inherent in a specific glassy environment. This complexity of partial crystallization and dissolution asks for homogenization of the crystalline phase within the glass matrix, as well as for additional thermal treatments as experienced during the drawing of the optical fiber, which was realized via employing a glass matrix with lower melting, and vitrification temperature, compared to pure silica [3]. Special attention should also be paid to the chemical stability of the crystal in its respective environment, which depends on its composition and, thus, its tendency to recrystallize, as has been noted for RE orthophosphate crystals [7].

Researchers have started working on an alternative approach involving the independent preparation of the active crystals and the glass to maintain a homogeneous distribution of NCs and matching their refractive indexes (see Fig. 1). Recently, we published an optical fiber with YPO_4:Pr^{3+} NCs embedded into phosphate-based glasses where luminescence and microscopic analysis proved NCs presence in the fiber core [11]. This approach, also termed glass powder doping, allows core materials (active NCs and matrix glass powder) to be mixed at room temperature. After an optional sintering step, the preform is directly drawn into a fiber using the powder-in-tube method. Glass powder doping can be applied to a larger variety of core material combinations, facilitating refractive index matching for the two constituents. It also promises better control of the size, crystal phase, and concentration of the active NCs, if they survive the drawing process.

This article presents results on optical fibers incorporating YPO_4:Yb^{3+} NCs. The synthesis procedure can be tuned to obtain different sizes and morphology. YPO_4 xenotime tetragonal structure can incorporate any rare-earth ion up to 100 %. Unfortunately, relatively high phonon energy discards this host lattice for some potential laser transitions.

Attention is also paid to the technological aspects that lead to discontinuities in the optical fiber core, resulting from viscosity changes in the core region analyzed by introducing ruby (Al_2O_3:Cr^{3+}) NCs. A strategy that facilitates the stabilization of the NCs against dissolution during the drawing process is presented. Furthermore, the fabricated fiber is characterized in terms of optical quality and emission in the 1 μm spectral range. The on/off gain of the NC-containing fiber is experimentally estimated. Refractive index matching and improvements of optical scattering losses are also discussed.

2. Experimental

2.1. NCs preparation

YPO_4:Yb^{3+} NCs with tetragonal crystal structure and Yb^{3+} concentration of 2 mol. % and 10 mol. % were synthesized using the following two methods based on a previously described co-precipitation method by Veber [12], and the adapted solvothermal method as described below.

2.1.1. Precipitation method

Stoichiometric amounts of $Y(NO_3)_3$ and $Yb(NO_3)_3$ were dissolved in deionized water. Twice, the stoichiometric quantity of $NH_4H_2PO_4$ was added while stirring at room temperature (RT). After 20 min, the precipitate was collected by centrifugation, washed three times with deionized water, and either resuspended in ethanol or dried overnight at 70 °C. To avoid the formation of the hydrated phase, the sample underwent thermal treatment at 900 °C for 2 h, with a heating rate of 10 °C/min. The particles reveal a broad size distribution from about 300 nm (round) to elongated shape with typically 500–1500 nm length. The obtained YPO_4:Yb^{3+} NCs were used as obtained.

2.1.2. Solvothermal method

A solvothermal method was used to synthesize YPO_4:Yb^{3+} NCs. $Y(NO_3)_3$ and the corresponding stoichiometric amounts of $Yb(NO_3)_3$ were dissolved in deionized water, followed by the addition of twice the stoichiometric amount of $NH_4H_2PO_4$. The mixture was stirred at RT for 5 min before being transferred to a Teflon-lined stainless-steel autoclave. The autoclave was then heated up to 180 °C at a rate of 10 °C/min for 24 h. The heating was then turned off, and the system was left overnight for cooling down to RT. Afterwards, the solid was separated via centrifugation, washed twice with deionized water and once with ethanol, and dried at 80 °C overnight. Subsequently, the powder was calcined at 1200 °C for 3 h. The particle size is in the order of 100–200 nm.

Additionally, to these samples, Al_2O_3: Cr^{3+} (ruby) nanoparticles

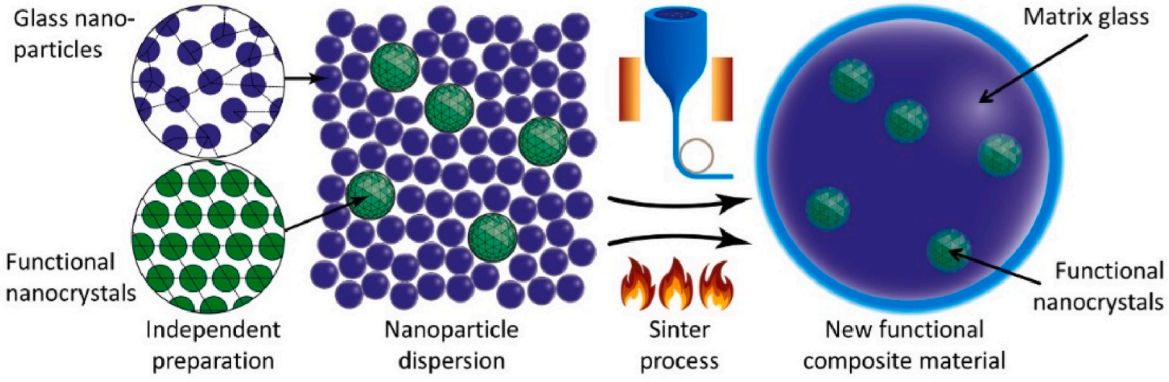

Fig. 1. Schematic of NCs doping fiber technology.

(99.99 %, 4N) were commercially available from MSE Supplies. Nominally high purity alpha aluminum oxides nanoparticles contain a significant amount of Cr^{3+} impurities (a few hundred ppm) with an average size of 100 nm. This material was structurally and spectroscopically characterized. We performed tests by mixing these nanoparticles with the corundum structure and the glass powders.

2.2. Matrix glass preparation

2.2.1. Matrix glass

Ohara S-NPH7 glass (Ohara, Japan), a niobium-rich phosphate glass, was selected as the material for the optical fiber's core embedding YPO_4: Yb^{3+} NCs. The choice of the core fiber was based on its optical properties, its refractive index ($n_{S\text{-}NPH7}$: $n = 1.778$ vs. n_{YPO4}: $n_o = 1.657$, $n_e = 1.838$), and transmission (0.998 at $\lambda = 1060$ nm). The second criterion was focused on the thermal properties, i.e., vitrification temperature ($T_g = 569$ °C), viscosity (T7.6 = 630 °C), and thermal stability of the glass concerning undesired crystallization [13]. An important aspect was the resistance of the glass to crystallization in the presence of nanocrystals, which was confirmed in preceding tests for the concentration regime of interest.

2.2.2. Matrix glass powderization

Bulk Ohara S-NPH7 glass of dimensions 100 × 50 × 10mm was milled using a high-energy ball mill (Retsch E-max, Germany) and following a two-step procedure described before [11], including one step at 650 rpm for 10 min using 10 mm zirconium oxide balls, and a subsequent step using 1 mm zirconium oxide balls at 1200 rpm for 10 min. Both steps were realized in a zirconium oxide 125 ml grinding jar at a filling level of 50 %. Particles of glass powder in the 550–1200 nm range were obtained. Then, glass powders were mixed with NCs [11].

2.2.3. Preparation of glass-NC mixtures

To avoid NC clustering and ensure sufficient optical quality of the fibers, the mixing process of the corresponding amount of NCs and core glass powder (with a weight ratio of NCs to glass ranging from 2–7 mg to 1 g, respectively) was tested using two different mixing methods a priori:

a) Ultrasonic mixing of powdered glass with NCs (1–2 g) in suspension (ethanol, 10–20 ml) using the VCX-500 sonicator (Sonics company, USA) with a time, amplitude, and maximum power of 5 min, 50 % and 500 W, respectively.
b) Mixing of dry powders in a ball mill (PM400, Retsch GmbH, Haan, Germany, grinding beaker: agate) with a maximum speed of 220 rpm/5min.
c) For the improvement of the homogeneity, a combination of mixing in a Speedmixer® (Hauschild GmbH, Hamm, Germany) in moist state with a maximum speed of 2000 rpm/2 min and subsequent drying, followed by the ball mill procedure mentioned above was chosen.

2.3. Preform preparation and fiber drawing

All powder mixtures were pre-sintered to a free-flowing powder with an enhanced powder density or to pellets for later use in powder-in-tube or "sintered body-in-tube" (stack of pellets like rod-in-tube, after pressing separately) preform arrangements. Previous experiments showed that ca. 30 % or less powder densities lead to tremendous problems during fiber drawing. Pellets were also used for initial material tests, such as NCs survival in the glass matrix and crystallization tendency evaluation. Those results determined the sintering parameters of preform material and conditions (dwell time) for drawing optical fibers. To get an aspired optical quality of the fibers, preforms were prepared from pre-sintered mixtures of S-NPH7 and NCs. The powder mixtures were densified by a pre-sintering step at 615–625 °C/10 min followed by pressing by hand (pressure <2 MPa) for core diameter smaller than 3 mm or by Cold Isostatic Pressing (CIP, EPSI system, $P = 250$ MPa) for $d_{core} \geq 3$ mm followed by pre-sintering 620 °C/30min, respectively. The resulting core material densities in the preforms are between 40 % and 60 % in the case of powder-in-tube (ref. fibers C1-C4, Y1, Y2 – Table 1) and 90 % in case of "sintered body-in-tube" (ref. Y3, Table 1).

For all preforms, the cladding material (Duran®, Schott) was used as it exhibits greater thermal resistance, i.e. the viscosity shifted towards higher temperatures (T7.6 = 825 °C) in relation to the core glass and no tendency to crystallize. Commercial tubes with dimensions (outer/inner diameter/wall thickness) of 9 mm/3 mm/3 mm and 8 mm/2.2 mm/2.7 mm were used for the fiber cladding [14].

Two partners, Leibniz-IPHT in Germany and AGH-BUT in Poland, performed optical fiber fabrication to derive critical aspects of this process. The drawing facilities differ in possible preform feed rates, maximum drawing speed, and temperature range with optimized control of the furnace. At IPHT, optical fiber drawing was carried out on the 10-m-high tower with a high-temperature Centorr furnace, and at AGH-BUT on the 8-m-high tower with a dedicated low-temperature furnace, that enables to optimization of the heating zones of the process, whereas the viscosity of the core glass was determined via hot stage microscopy. As it turned out, the viscosity parameter is also influenced by the percentage content of the NCs dopant. It was analyzed using the examples of optical fibers doped with Al_2O_3:Cr^{3+} crystals discussed further in this paper.

2.4. Analysis methods

2.4.1. Structural analysis (XRD, TEM, EDS)

X-ray diffraction (XRD) using a D8-Advance and D2 (Bruker), using a Cu tube ($\lambda = 1.5419$ Å) was used to determine the crystalline YPO_4 phase as well as to estimate the average NCs size through Rietveld refinement from the diffraction peak width. The XRD size was compared with the size obtained from TEM images (JEM1011, JEOL).

For the proof of the survival of NCs and unwanted secondary crystallization, the X-ray diffraction (XRD, device X'pert Pro, Malvern Panalytical, Almelo, The Netherlands, CuKα radiation, the ICDD database) as well as Transmission Electron Microscopy (TEM) including local EDS element analysis were carried out. For the chemical analysis and nano-structure characterization of the fibers TEM lamellae were prepared using a Dual Beam SEM-FIB system (Carl Zeiss NVision 40) and imaged using a scanning TEM (Carl Zeiss Libra 200 MC Cs) at an accelerating voltage of 200 kV; element analysis of the lamellae was performed using energy dispersive X-ray spectroscopy (EDS) in TEM.

Despite long-term measurements (overnight), the XRD method reaches its limits because of the low NCs/crystalline phase content in the analyzed fiber samples, including the cladding material. The superposition of both materials leads to XRD spectra with a prominent amorphous background that impedes accurate identification of the

Table 1
Active fibers consisting of S-NPH7 phosphate matrix glass and Al_2O_3:Cr^{3+} in DURAN tube (8 × 2.2 mm^2 outer and inner diameter) to investigate the influence of NCs amount.

No.	Al_2O_3: Cr^{3+} NCs	Drawing Parameters Temp./preform feed speed/fiber tension	Results
C1	3 wt % 2.5 vol%	1070–1110 °C 0.95–1.8 mm/min 1770 mN	transparent fiber pieces, losses: 25 dB/m, diameter: 125 μm
C2	5 wt % 4.2 vol%	1080–1110 °C 1.0–1.3 mm/min 1620 mN	fractures, amorphous fluorescence, reduced lifetime, stable process at 1100 °C, diameter: 125 μm
C3	7 wt % 5.9 vol%	1080–1110 °C 1.0–2.1 mm/min 830 mN	fractures, amorphous fluorescence, reduced lifetime, diameter: 125 μm
C4	10 wt % 8.5 vol%	1080–1120 °C No stable process –	No sufficient viscous flow, only short fiber pieces of >500 μm diameter

crystalline phases. Therefore, fluorescence spectroscopy was an integral method of choice to prove the survival of YPO_4:Yb^{3+} NCs.

2.4.2. Structural analysis (fluorescence spectroscopy)

Spectroscopic measurements of NCs were carried out in a FLS920 spectrofluorometer (Edinburgh Inst.). The system is equipped with double monochromators for emission and excitation measurements. Three PMT covering emission in the 300–1600 nm range are coupled to the emission arm.

In an alternative setup (Fig. 2a), pump light is focused through the cladding into the fiber core, and the fluorescence signal is collected by a 400 μm collecting fiber transversally oriented to the sample fiber. Using double-transversal pump probe technique, the sample fiber can be axially shifted to measure the fluorescence signal at different fiber positions, minimizing longitudinal absorption effects. The collected signal is measured by a fiber spectrometer (Spectro 320D) equipped with a cooled PMT.

The homogeneity of the fibers with respect to the spatial NCs distribution was investigated by transversal fluorescence spectroscopy at different positions along the fiber (Fig. 2a) and optical microscopy (Fig. 2b). The setups for the fluorescence measurements at AGH-BUT (λ_{exc} = 940 nm, StellarNet Green-Wave spectrometer) and IPHT (λ_{exc} = 950 nm, Spectro 320D spectrometer) differ slightly concerning measured fiber core volume and influence of cladding glass however led to very similar results.

3. Results

3.1. Fiber core uniformity

3.1.1. Influence of particle concentration induced viscosity increase on fiber drawing

During fiber-drawing, the preform is heated up to achieve a viscosity compatible with the drawing process. The glass viscosity primarily determines the drawing temperature. However, the preform comprises three distinct components – glass powder, NCs, and Duran glass cladding – each with unique thermophysical properties, which complicate the fiber-drawing process. Clusters of crystallites or regions with significantly higher NC concentrations than the average in the core glass can disrupt the viscous flow of the core material, resulting in irregularities in the fiber core's geometry and composition. Consequently, it is crucial to first evaluate the impact of particulate NCs on viscosity during the fiber-drawing process.

The influence of dispersed solid particles on the viscosity of a liquid is well-known in the context of suspensions. The relationship between solid-phase fraction and viscosity is A schematically in Fig. 3a. Generally, the viscosity increase arises from the disruption of the liquid's flow profile by the dispersed particles. For highly dilute suspensions, where particle concentrations are low (up to approx. 5 vol%) and particle-particle interactions are negligible, the Einstein relation [15] can describe the influence of the solid volume fraction, Φ, on the viscosity, η: $\eta_{susp} = \eta_{fluid}(1 + 2.5\Phi)$. At higher particle concentrations, particle-particle interactions result in a non-linear dependency between viscosity and solid volume fraction. This behavior can be expressed using equation such as: $= \eta_{fluid}(1 + a\Phi + b\Phi^2)$ [16]. Understanding these relationships is critical for predicting and controlling the viscosity of NC embedded into the glass matrix during fiber production.

The deformation (flow) of such a system requires increasingly higher shear stresses as the particle concentration increases. In our material system, there might be secondary crystallites besides the NCs, contributing to the observed increase in viscosity. This effect is particularly relevant in cases in cases of particle aggregation, where a higher local NCs concentration promotes an increased nucleation rate for secondary crystallization. Conversely, the cladding material (Duran), which constitutes the largest volume fraction in the preform, governs the tensile stress during fiber drawing experiments, being too low to deform the core material uniformly, resulting in locally different kinetic conditions. When the viscosity of the core material exceeds that of the cladding material, confinement or interruptions of the core material flow within the fiber can occur. An example of such interrupted core material flow is shown in Fig. 3b (10 wt % ruby NCs (8.5 vol%), see below).

3.1.2. Influence of nanoparticle concentration induced change in liquidus temperature on fiber drawing (solubility of NCs)

According to phase relations, the liquidus temperature (maximum temperature below which a crystalline phase and a melt coexist based on phase composition) in a system liquid/melt-solid/crystal system depends on the concentration of the crystalline phase. In Ref. [18] the solubility of RE orthophosphates ($REPO_4$) in $Pb_2P_2O_7$ melt was investigated within the range of 10–20 mol. % $REPO_4$ (corresponding to ca. 3.4–7.2 wt % YPO_4). The study revealed a concentration dependence decrease in liquidus temperature of about 50 K per wt. % $REPO_4$. In inhomogeneous powder mixtures, local concentration deviation, therefore, could lead to an inhomogeneous presence of surviving NCs or formation of secondary crystallites.

To assess the significance of the dependency between NC solubility and concentration under the fast, non-equilibrium conditions of the fiber-drawing process, a series of test fibers was prepared. These fibers featured composed of Al_2O_3:Cr^{3+} NCs (ruby, average size: 100 nm, MSE Supplies LLC, Tucson, USA) embedded in an S-NPH7 matrix glass within DURAN tubes. NCs concentrations ranged from 3 to 10 wt % (2.5–8.5 vol %) as detailed in Table 1. Ruby was chosen because Al_2O_3 is absent in the core glass composition, that may speed up dissolution processes, while also enabling differentiation between the amorphous and crystalline environments of Cr^{3+} ions. Al_2O_3:Cr^{3+} NCs exhibit a characteristic sharp-line emission at 694 nm associated with the spin-forbidden $^2E \rightarrow {}^4A_2$ transition with minimal scattering losses expected due to the small refractive index mismatch. In contrast, Cr^{3+} in the glassy matrix

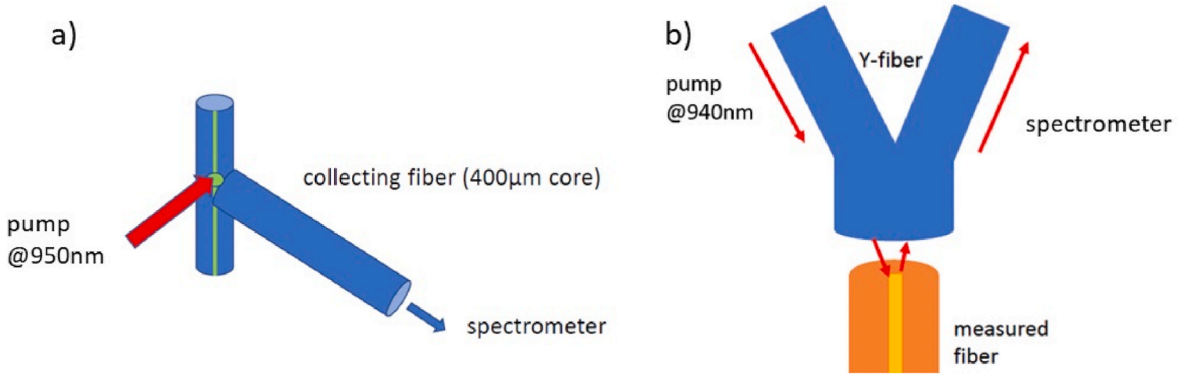

Fig. 2. Schematic of setups of the fluorescence measurements in a) IPHT and b) AGH-BUT.

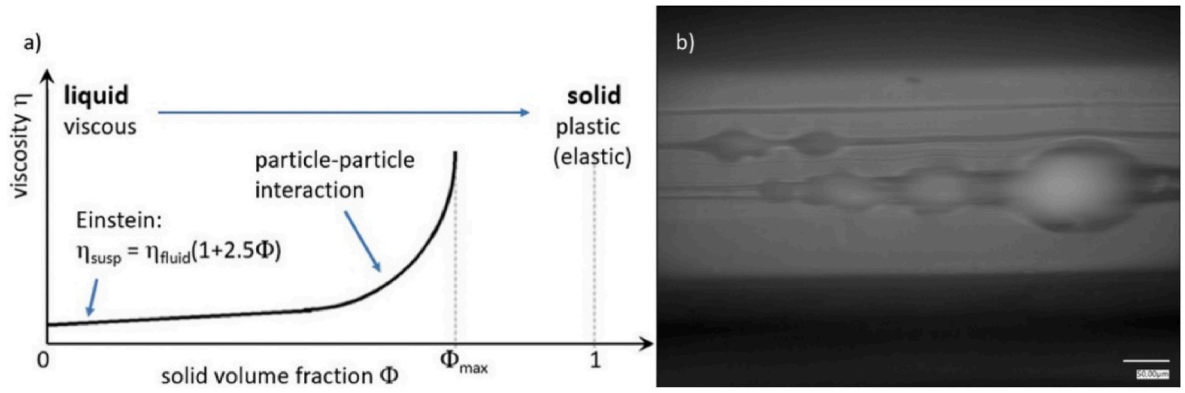

Fig. 3. a) Influence of the solid volume fraction on the viscosity of a suspension (modified from Ref. [17]), b) Side view of a fiber core with interrupted material flow due to 10 wt % ruby NCs content (image about 550 μm wide).

induces broadband emission above 700 nm, associated with the spin allowed $^4T_2 \rightarrow {}^4A_2$ transition. For this series, the initial fiber-drawing parameters (drawing temperature, preform feed rate) were optimized using core material mixtures with 3 wt % NCs in the same tube dimensions (8 × 2.2 mm^2 outer and inner diameter), as shown in Table 1. To enhance powder density within the preform, all powder mixtures were pre-sintered at 620 ± 5 °C before the drawing process.

In the NCs concentration-dependent experiments, it was observed that a drawing temperature of 1100 ± 10 °C combined with a feed rate between 1.0 and 1.5 mm/min resulted in a stable drawing process, characterized by minimal fiber diameter fluctuations) for fibers C1-C3. Lower drawing temperatures and higher speeds increase viscosity and shear stresses, enforcing secondary crystallization or disrupting the drawing process. Despite the unknown spatial distribution (i.e. local concentration) of the NCs in the powder mixture, differences in the average NC concentration (ca. 3, 5, 7, and 10 wt % NCs) showed clear trends in XRD investigations (Fig. 4). The 3 % NC-fiber (C1) displayed an amorphous XRD pattern, suggesting significant dissolution of NCs, which contributed to optical quality sufficient for loss measurements (ca. 25 dB/m). In contrast, the 5 % NCs fiber showed tiny shoulders and peaks in its XRD pattern, corresponding mainly to sodium potassium niobate $Na_{0.9}K_{0.1}NbO_3$ (reference file 98-001-5365) or sodium niobate $NaNbO_3$ (98-000-7690). The presence of corundum (Al_2O_3, 98-001-6925 representing the ruby NCs structure, was inconclusive. With

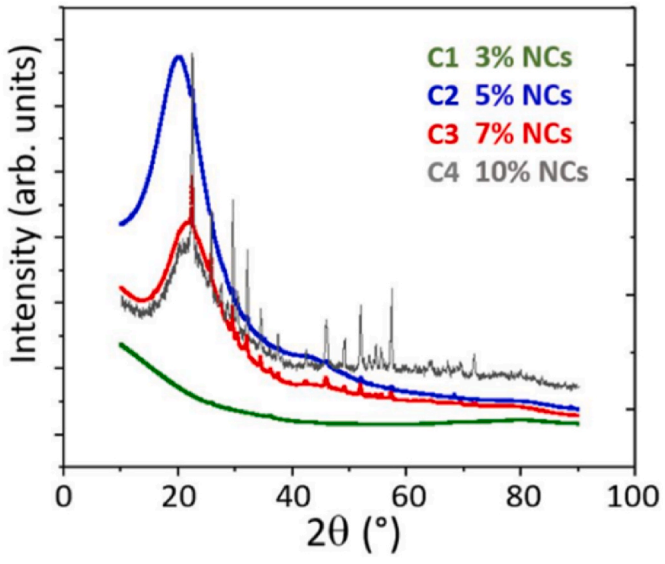

Fig. 4. XRD pattern of milled fibers (including DURAN cladding) prepared with ruby NCs.

increasing NCs concentration, a rise in the crystalline phase content was evident. The 7%NC-fiber exhibits a mixture of crystalline phases, including of sodium potassium niobate, rutile (TiO_2), and other unidentified phases. However, the 10 wt % NC fiber experienced hampered viscous flow in the core material, resulting in an unstable drawing process and a thicker fiber diameter (~1 mm), indicating different kinetic conditions during cooling. XRD analysis of this sample revealed a phase mixture of niobates, again rutile and a small amount of Al_2O_3. The increased peak intensity and reduced peak-width indicated a higher crystalline fraction and larger size compared to the 7 % NC sample.

Since it was a testing example, the nucleation and growth mechanisms of the secondary crystallites were not investigated in detail. Besides, it remains unclear at what stage of the drawing process these crystallites form or whether the NCs act as nucleation agents. This question requires further exploration.

A similar effect of hampering the viscous flow was found in a test fiber containing 5 wt % YPO_4:Yb^{3+} NCs mixed using only a sonication process (par. 2.2a). The importance of the homogeneity of NCs depending on the mixing procedure can be seen in Fig. 5, showing cross sections of two different fiber cores: (a) with a dense cluster of NCs, whereas in the neighborhood of the cluster, no NCs can be identified (Fig. 5a); and (b) uniform distribution of spots with different breaking strength or mechanical stress due to the thermal expansion mismatch between particles and matrix indicating a uniform particle distribution (Fig. 5b) in fiber Y3 (further described). Fig. 5b (right) shows a SEM zoom onto the fiber cross-section. It is impossible to state whether this NCs distribution is only a result of the mixing procedure or influenced by any preferred dissolution of separated NCs in the low-concentration region of the fiber core.

3.2. *Powder-in-tube S-NPH7/YPO4: Yb^{3+} NCs fibers*

The influence of NC concentration in the glass matrix was also considered using the S-NPH7 glass embedded with 3 wt % (2.3 mol. %) and 7 wt % (5.5 vol%) YPO_4:Yb^{3+} NCs under constant tube dimensions (see Table 2). In fibers containing 3 wt % NCs (fiber Y1), no NC survival was observed across various drawing conditions, including preform feed rates of 0.9–2.8 mm/min, preform outer diameter of 8, 9, and 16 mm, and pre-sintering conditions tested despite the possibility of locally enhanced NCs concentration caused by a non-ideal mixing process.

A subsequent trial with an increased NC content of 7 wt % (fiber Y2), using identical tube dimensions and drawing parameters as fiber Y1, was carried out. XRD analysis of fiber Y2 revealed clearly the presence of YPO_4- in the fiber core (Fig. 6), with particle sizes of 100–200 nm), notably smaller than those in Y1 (500–1500 nm). The estimations crystallinity based on XRD data corresponded reasonably well with the expected content based on the of the initial composition. Additionally, a minor amount of a secondary crystalline phase, identified as rutile, was

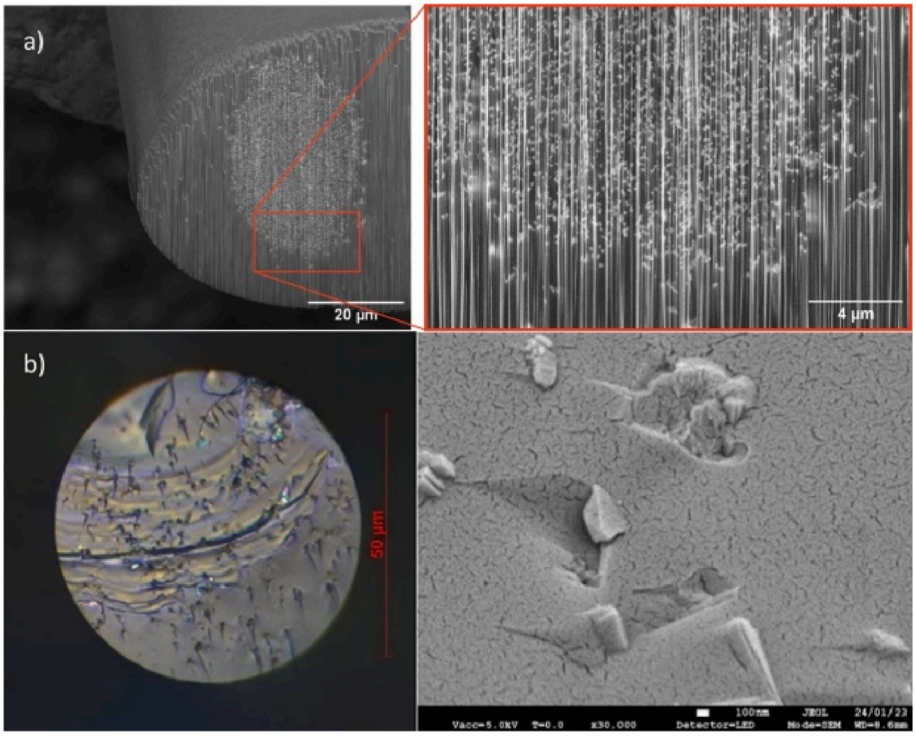

Fig. 5. a) Inhomogeneous NC distribution in a test fiber core after ultrasonic mixing of particles only (left) and vertical structures as a result of the SEM/FIB treatment of the fiber core (right), b) microscope image of the Y3 fiber core fractured surface showing uniformly distributed NCs (left) and SEM image of the Au sputtered fiber core cross-section showing separated crystals in a matrix (right, width of the image: ca. 3.7 µm).

Table 2
Particle-doped fibers consisting of S-NPH7 glass and $YPO_4:Yb^{3+}$ in DURAN cladding.

No.	$YPO_4:Yb^{3+}$ NCs	Mixing	Drawing Parameters Temp./preform feed speed/fiber tension	Results
Y1	3 wt % (2.3 vol %) (precipitation)	normal speed (par. 2.2b)	1070–1100 °C, 1.0–1.8 mm/min 1230 mN	amorphous fluorescence, reduced lifetime
Y2	7 wt % (5.5 vol %) (solvothermal)	high-speed (par. 2.2c)	1070–1110 °C 2.0–2.9 mm/min 1610 mN	**survival of NCs** (by XRD, fluorescence), very low transparency
Y3	7 wt % (5.5 vol %) (precipitation)	high-speed (par. 2.2c)	1000 °C (1 min), 1100 °C >7 mm/min 50 mN	**NCs survived** (by fluorescence, TEM, microanalysis)

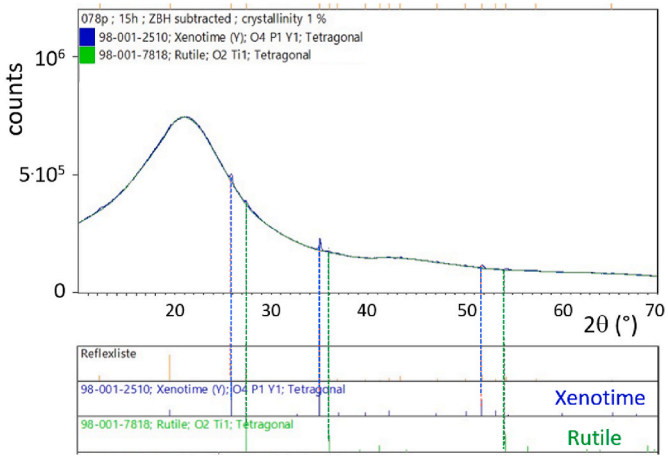

Fig. 6. XRD pattern of fiber Y2 showing a small amount of crystalline YPO_4 beside the dominating amorphous glass material upon processing of $YPO_4:Yb^{3+}$ in DURAN cladding.

also detected in the fiber core.

Fluorescence measurements confirm a crystalline signature of the Yb^{3+}-doped YPO_4 in the 7 wt % NCs-fiber Y2. The measured intensities fluctuate depending on the position, probably caused by bubbles. However, the crystalline character is always observed (Fig. 7a).

Fig. 7b contains normalized spectra from 2 different fiber positions and for comparison the spectrum of fiber Y1 (amorphous) with fully dissolved NCs. The Yb^{3+} emission is clearly different when Yb^{3+} is placed in the YPO4 NCs from that of Yb^{3+} in the glassy environment. In fiber Y2 (Fig. 7c), the lifetime of Yb^{3+} (730 µs) fits well with that of the as-prepared NCs (770 µs). The difference is about 5 %.

3.3. *"Sintered body-in-tube" S-NPH7/$YPO_4:Yb^{3+}$ NCs fiber*

According to previous successful experiments, the fiber drawing was carried out at the AGH-BUT facility, which allows a two-step heating procedure with dwelling time [11]. This fiber sample (Y3) was embedded with 7 wt % NCs, mostly with elongated shape with typically 500–1500 nm length, since the survival of NCs was more stable. The main aim was to improve the optical quality of the fibers containing the higher NCs percentage by adjusting drawing conditions. The core material was mixed using improved mixing methods. Compared to the drawing experiments at IPHT a much higher preform feed rate of >7 mm/min was used.

TEM studies investigated the survival of the NCs in the fibers as well. A microanalysis of the crystals was carried out to distinguish surviving NCs from possible secondarily formed crystalline particles apart from using fluorescence measurements. In fiber Y3, crystalline particles are observed (Fig. 8 a) whose composition corresponds roughly to YPO_4

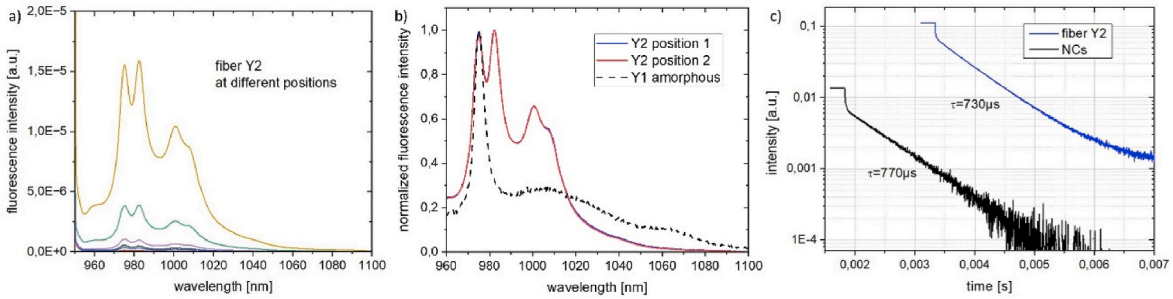

Fig. 7. Fluorescence spectra of fiber Y2 with 7 wt % NCs, a) measured at random fiber positions, b) normalized spectra of 2 random positions of fiber Y2 and fiber Y1 after complete dissolution of NCs and c) measured fluorescence lifetime of fiber Y2 indicating a crystalline Yb^{3+} surrounding and of the initial YPO_4:Yb^{3+} NCs.

with Yb^{3+} addition. Because of the superposition of the P Kα peak with the Y Lα peak and a limited energy resolution of the measuring system, the analyzed P amount is overestimated, and the molar Y/P ratio is < 1 (Fig. 8 b). Traces of matrix glass elements could be a result of the choice of the analyzed volume. The composition of the glass matrix is like that of the initial glass. A tiny amount of dissolved NCs was seen in the matrix composition.

Note that we used NCs that are characterized with large elongated NCs (length 500–1500 nm) prepared by precipitation method (Fig. 8a). In contrast, in later experiments, spherical NCs prepared by solvothermal procedure (mean size < ca. 150 nm) were incorporated in the glass (Y2). Initially, it allowed us to determine NCs localization in the core and the tendency to aggregation. Subsequent experiments revealed that fibers obtained using spherical NCs exhibited lower scattering losses i.e., better optical quality than fibers from precipitated bigger elongated NCs.

The 7 wt % NC-fiber (Y3), prepared with improved mixing techniques, revealed a homogeneous distribution of NCs (Fig. 9). The crystalline nature of YPO_4:Yb^{3+} was confirmed using TEM microanalysis (Fig. 9a), fluorescence spectra (Fig. 9b) and lifetime measurements (Fig. 9c). The fluorescence spectra showed similar intensities across different fiber positions, indicating a uniform NC distribution (active ion in the crystalline environment). The measured lifetimes were in good agreement with the literature values for YPO_4:Yb^{3+} and the lifetimes of the as-prepared NCs [19].

3.4. Optical quality

Despite the presence of surviving NCs, all fiber with embedded NCs in the cores suffered from high optical losses caused by scattering. Those losses were primarily caused by NCs aggregation and bubbles, as well as fractures initiated by thermal expansion coefficient mismatch of core and cladding glasses. This was proven by drawing fibers with completely dissolved NCs that exhibited obviously much less scattering and a better homogeneity concerning bubble formation, which in total was caused by an overall higher (better) viscous flow during drawing.

In conventional optical fibers, mechanical stresses are usually minimized by using cladding-core combinations with similar thermal expansion coefficients. In our fibers, the mismatch of the thermal expansion coefficients is of one order of magnitude (S-NPH7: $\alpha = 13.10^{-6}\ K^{-1}$, DURAN: $\alpha = 3.3.10^{-6}\ K^{-1}$) leading in bubble-free fibers to fractures of the core. Our experiments revealed that the core diameter is the crucial factor influencing fracture formation. For fibers with core diameters greater than 200 µm, irregular fracture planes were observed in all directions, with core material fragments between 50 and 150 µm (Fig. 10a). In thinner fiber cores (ca. 50 µm or less), fractures were confined to radial directions (Fig. 10b). The axial distance between fractures in a 50 µm core was up to 100 µm, whereas cores with diameters around 28 µm-core exhibit fracture distances in the millimeter range (Fig. 10c). We expect further improvements, with fracture distances of some decimeters for core diameters of ca. 10 µm. To produce fibers with such small core diameters, cladding tubes with adjusted diameter-wall thickness ratios are necessary that were not commercially available.

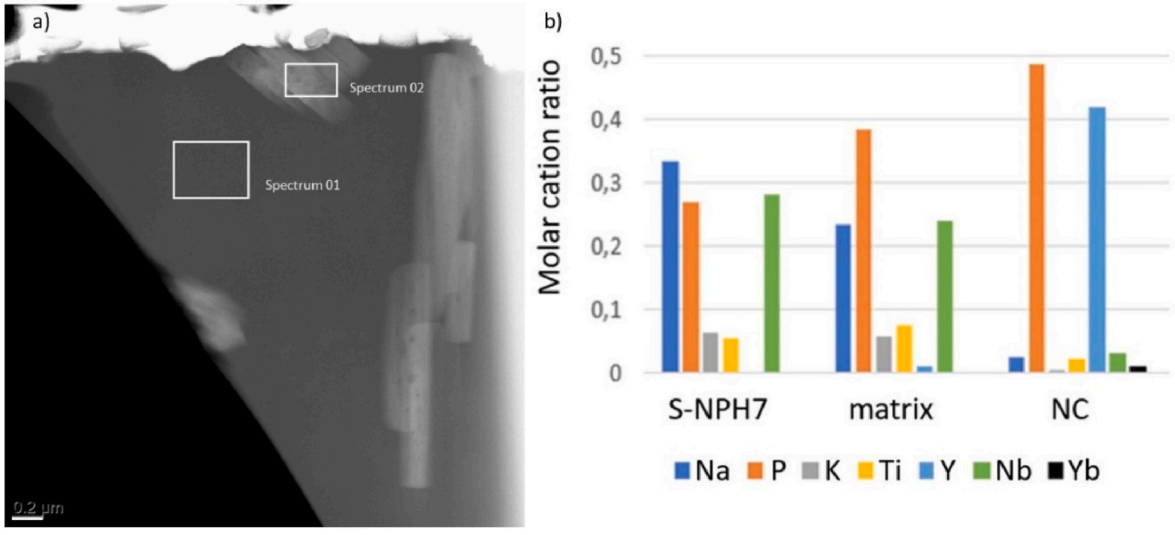

Fig. 8. a) STEM dark field image of a lamella with the marking of analyzed area of fiber core Y3 (scale bar: 0.2 µm) and b) molar cation content normalized to the sum of cations of the initial glass S-NPH7, the core glass matrix and NCs of fiber Y3.

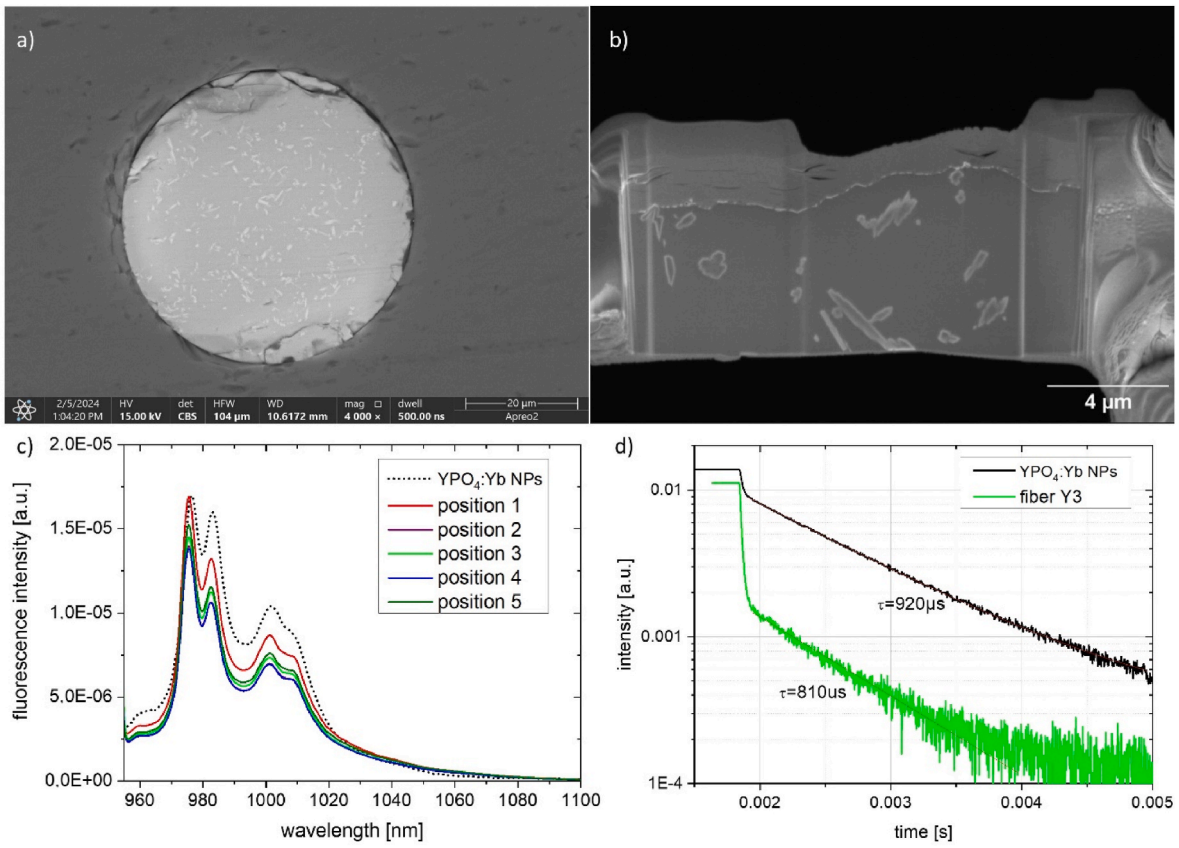

Fig. 9. Homogeneity of NCs distribution in Y3 fiber sample a) SEM image of the fiber core (scale bar 20) µm and b) TEM lamella (scale 4 µm), c) fluorescence spectra of YPO_4:Yb^{3+} NCs and along the fiber at different positions, d) lifetime measurement of the fiber and the initial NCs.

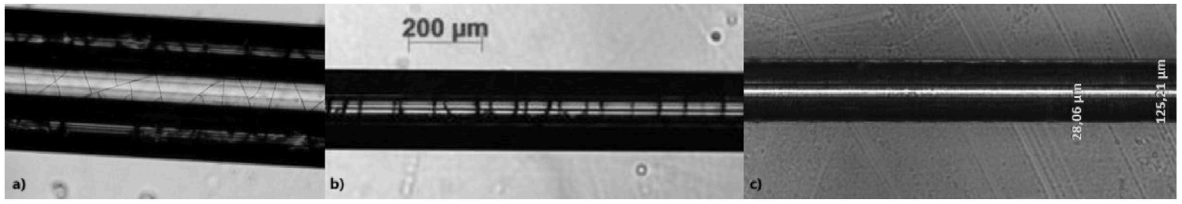

Fig. 10. Side view of S-NPH7/DURAN-fibers (core/cladding) with YPO_4:Yb^{3+} doping with different core diameters (a) ca. 200 µm, b) ca. 50 µm and c) 28 µm) and fracturing behavior of the cores.

3.5. Optical loss

A 1.2 cm long fiber (Y3) with surviving NCs (S-NPH7 glass with YPO_4:Yb^{3+} NCs (7 %) and no bubbles or breaks was chosen for a loss measurement. Care was taken to minimize the impact of light guided in the cladding by selectively collecting the core light at the fiber end with an additional fiber of similar core diameter and stripping the cladding light. The reference measurement was performed in the air because the fiber length is too short for a cut-back measurement. Therefore, the loss coefficient in Fig. 11 contains a small contribution of the fiber coupling losses which can be neglected when compared to the propagation losses. Nevertheless, the loss is much higher than the intrinsic loss of the matrix glass S-NPH7, which is about 1 dB/m near 1 µm wavelength, according to the transmission data from the datasheet. This fact and the loss curve's spectral shape suggest that the losses are mainly due to scattering processes. These losses are much higher than the productive Yb absorption peak near 1 µm wavelength and require further discussion.

Nanoparticle-doped materials suffer from scattering losses depending on the particle size and density, as well as the difference of the refractive indices of the matrix n_m and the nanoparticle n_n. For spherical

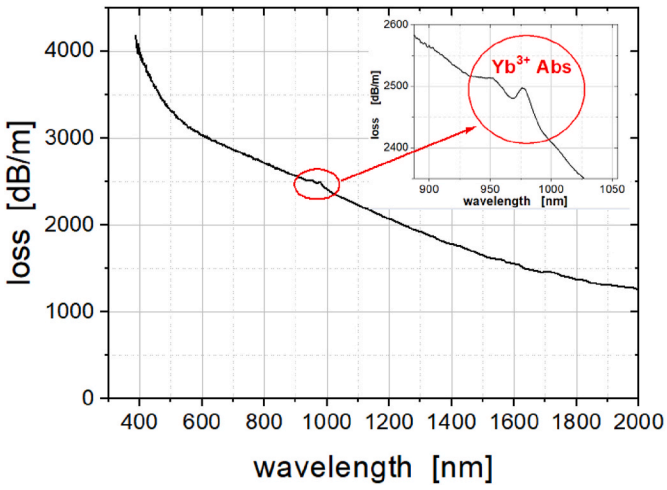

Fig. 11. Loss measurements of fiber Y3 with survived YPO_4:Yb^{3+} NCs.

NCs in an optical fiber, the scattering losses can be estimated by [9].

$$\alpha_{Rayleigh}[dB/m] = 4.34*\frac{(2\pi)^5}{48}*N*\Gamma*\frac{d^6}{\lambda^4}*n_m^4*\left(\frac{n_n^2-n_m^2}{n_n^2+2n_m^2}\right)^2 \quad (1)$$

with the diameter d and the number density N of the NCs, the overlap factor Γ between the optical field and the scattering core. For the very strong dependence on the NCs diameter, one needs to understand that the size reduction also reduces the NCs volume. In the present situation, it is desirable to express the scattering losses in terms of the NCs volume fraction F (instead of the number density N)

$$F = \frac{V_{NC}}{V} = N\frac{\pi}{6}d^3 \quad (2)$$

The scattering losses are now

$$\alpha_{Rayleigh}[dB/m] = 8.29*\frac{(2\pi)^5}{48}*F*\Gamma*\frac{d^3}{\lambda^4}*n_m^4*\left(\frac{n_n^2-n_m^2}{n_n^2+2n_m^2}\right)^2 \quad (3)$$

For non-spherical NCs shape, the scattering losses will be different, but the basic scaling laws for the NC size $\sim d^3$ and the refractive index contrast $\sim(n_n\text{-}n_m)^2$ should still hold and provide the most efficient routes for mitigating scattering losses.

In our case, the NCs are still large-sized (see 2.1), resulting in large scattering losses. In terms of the refractive index matching, the matrix glass index is $n_m = 1.7542$ at 852 nm, which is quite close to the YPO_4 average refractive index of 1.732 at that wavelength [20]. However, YPO_4 has a very large birefringence with ordinary and extraordinary refractive indices of $n_o = 1.643$ and $n_e = 1.82$, respectively. This situation is not ideal because the scattering loss will depend on the orientation of the NCs concerning the fiber axis, and refractive index matching can only be achieved for an ensemble of NCs with a correct orientation. The selection of NCs with low or no birefringence is advantageous or otherwise, the mitigation of scattering loss must be addressed mainly by NC size reduction.

3.6. Splice development

The splicing to silica fibers is an important step because it provides access to a wide range of fiber-optic components. For this purpose, a splice of the fiber C1 with a standard Corning HI-1060 fiber was developed using a Vytran GPX-3200 splicer with resistive heating filaments made of graphite. Due to the very different thermomechanical properties of the two fibers with softening temperatures about 1000 K apart, an asymmetric splice arrangement was chosen, where the filament is placed off-center to selectively heat the more temperature-resistant silica fiber. Successful splicing could be obtained by adjusting the offset, splice power and duration (Fig. 12).

3.7. Estimation of on/off gain

Despite the dominating scattering losses, an experiment was conducted to demonstrate the potential of the NC-doped fibers for optical gain. The Y3 fiber sample of 1.2 cm length was pumped at 976 nm wavelength and a seed wavelength of 1009 nm in the fluorescence band of the YPO_4:Yb^{3+} NCs was chosen. The optical on/off gain was measured by comparing the signal output power with and without pump power applied to the fiber core.

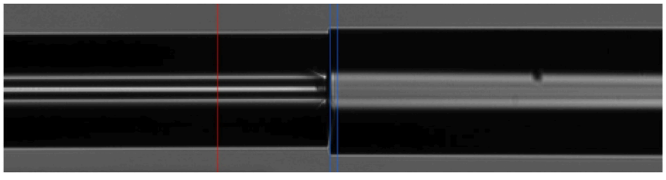

Fig. 12. Splices between fiber C1 (left) and a standard silica HI-1060 fiber (right).

The setup for this gain measurement is shown in Fig. 13. Both lasers are single-mode diodes with polarization-maintaining (PM) fiber termination that are combined by a polarization fiber combiner. This combiner enables seeding and pumping of the NC fiber core from one delivery fiber. Due to the short fiber sample length, butt-coupling was again chosen. The adjustment of the light-coupling was realized with high-precision translation stages. The core area of the fiber end facet was imaged onto the detector surface of a power detector (Thorlabs S122C) using a lens such that any cladding light bypasses the active detector area.

For the amplification measurement of the 1009 nm seed signal, the residual power of the pump light and part of the amplified spontaneous emission (ASE) was blocked by a high pass filter (FELH1000), which is highly transmitting at >1000 nm. To avoid any influence of residual pump light passing through the filter during the gain measurement, the power behind the filter was measured without any seeding for the entire power range of pumping. These values correspond to leaking pump power as well as ASE.

For investigating the gain of the NC-doped fiber, 7 mW of seed power @ 1009 nm were coupled to the active fiber core. The collimated transmitted signal power behind the lens without pumping was measured at 135 μW.

Additional core-pumping at 976 nm slightly enhanced measured output power @ 1009 nm seed wavelength. To avoid any contribution from pump power leaking through the filter, the before measured residual powers were subtracted without any seeding behind the long pass filter. This is a conservative estimate, because not only residual pump power but also ASE are subtracted. The output characteristics are shown in Fig. 14.

The resulting output power of 180 μW corresponds to a signal amplification of 33 % or 1.25 dB with respect to the unpumped fiber. The gain coefficient is about 1 dB/cm or 100 dB/m. The NCs of the evaluated fiber had a relatively low Yb-concentration of 2 mol. % compared to a recent study (to be published elsewhere) of YPO_4 NCs showing low quenching effects up to even 20 mol. % Yb^{3+} using starting precursor with 4N purity, which raises the assumption that even more gain would be possible with higher Yb-doped NCs.

Even though these gain coefficients fall significantly short of the estimated loss coefficients, this is the first experimental evidence that relative gain coefficients larger than 100 dB/m can be achieved, especially if NCs with higher Yb^{3+} doping (e.g. 10 or 20 at%) are used. However, a drastic reduction of losses is required to achieve a net gain.

4. Discussion and summary

We have extensively investigated the use of glass powder doping for producing NC-containing fibers, where the laser-active NCs survive the fiber drawing process. This method allows good control over size, crystal phase, and concentration of the NCs as well as the possibility of achieving refractive index matching with the matrix glass. This powerful approach still faces significant technological challenges in this early stage, several of which are addressed in this study.

We realized materials by incorporating externally synthesized functional nanocrystals into a glass matrix and their survival in the fiber drawing process. Embedded rare-earth-doped NCs also provided a good indication of the local environment and thus the survival of the NCs. The matrix material was chosen with respect to the refractive index of the NCs, thermomechanical properties (softening behavior) of the fiber cladding material and its tendency to crystallization. One key issue for the survival of NCs is the optimization of the NCs content in the core material: low enough not to hamper the viscous flow during the drawing but high enough to ensure a minimum liquidus temperature of the NC glass-melt system. The optimization needs to be achieved not only on average but along the fiber, stressing the importance of a good NC-glass powder mixing procedure. This strategy for the survival of the NCs

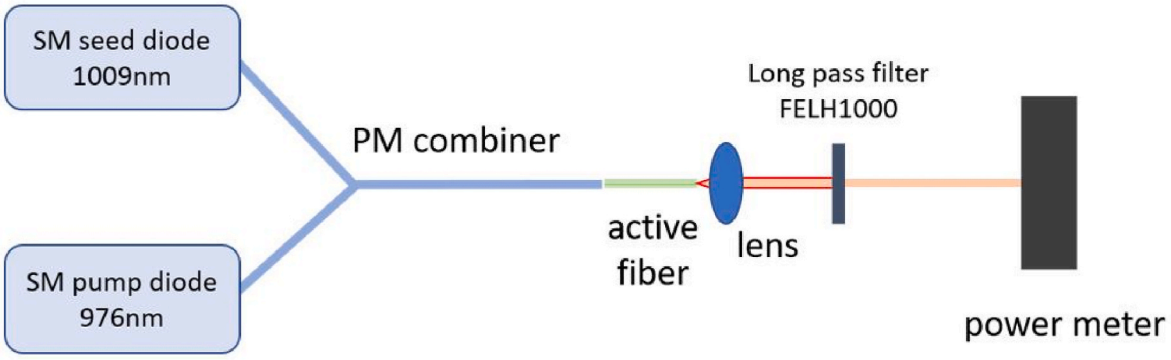

Fig. 13. Setup for signal amplification in a NC doped fiber.

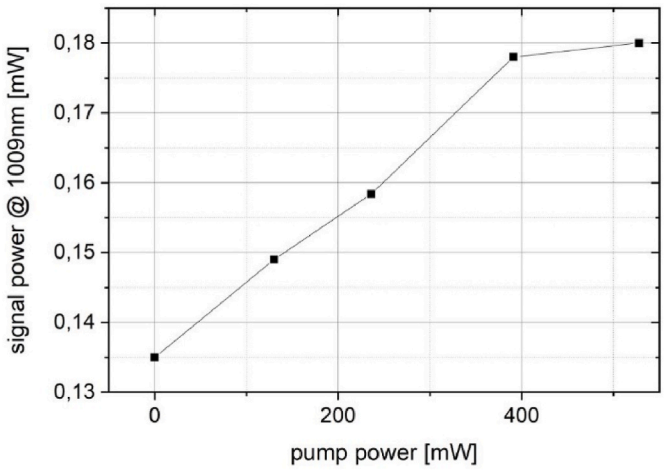

Fig. 14. Amplification experiment showing the signal output power vs. coupled pump power.

appears to be effective for other NC materials as well because it has been successfully demonstrated for both YPO_4:Yb^{3+} and Al_2O_3:Cr^{3+} NCs. The dominant factor for survival of NCs under comparable powder-in-tube drawing conditions seems to be the NCs content. Otherwise, compared with the two-step heating ("sintered body-in-tube"), the duration of diffusion (unwanted dissolution process) depends strongly on the preform speed rate and drawing speed, respectively, at the maximum drawing temperature. The NCs preparation method with the given NC sizes seems not to be the most important parameter.

Our experiments show that steps to increase the solid phase content in the fiber preform like pre-sintering and pressing the NC-glass powder mixture are necessary for a stable drawing process and reducing bubbles in the fiber. The use of reducing atmosphere or vacuum is limited if the core material contains polyvalent ions. In our fibers, a correlation between the core diameter and frequency of fractures in the core (i.e. the thinner the core the less fractures) could be caused by the mismatch between the thermal expansion coefficients of the core and cladding glass. Nevertheless, defect-free short fibers were prepared and characterized optically and spectroscopically.

For practical applications, the optical quality of the fibers needs to be significantly improved. Apart from reducing the frequency of fractures by using preform geometries leading to smaller core diameters, the reduction of optical scattering losses is most important. While YPO_4-based NCs are non-ideal due to their considerable birefringence, we have demonstrated that refractive index matching of the NCs can be achieved with suitable multi-component matrix glasses. The other effective route to lower scattering losses is the NC size reduction, which is quite feasible as smaller NCs (150 nm) have also survived the drawing process. We demonstrated a relatively large on/off gain coefficient of about 1 dB/cm, however, which will only become relevant once the scattering losses have been successfully mitigated.

Furthermore, secondary crystallization can be avoided using optimized matrix glass compositions. It must be noted that the commercial glasses employed in this study have not been developed and optimized for the purpose of glass powder doping.

This publication investigates glass-powder-doped fibers in the context of fiber lasers and amplifiers. It is one of the most challenging applications because it requires a large active volume fraction for high gain and is very sensitive to propagation losses. However, the experimental results and learnings are also applicable to other materials and applications, particularly for less demanding fiber sensors.

CRediT authorship contribution statement

Dominik Dorosz: Writing – review & editing, Writing – original draft, Supervision, Resources, Methodology, Investigation, Formal analysis, Conceptualization. **Marcin Kochanowicz:** Writing – review & editing, Methodology, Investigation, Conceptualization. **Rafael Valiente:** Writing – review & editing, Writing – original draft, Supervision, Methodology, Investigation, Formal analysis, Conceptualization. **Robert Müller:** Writing – review & editing, Writing – original draft, Methodology, Investigation, Conceptualization. **Andrea Diego-Rucabado:** Resources, Investigation, Data curation. **Fernando Rodríguez:** Methodology, Investigation. **Nuria Siñeriz-Niembro:** Methodology, Data curation. **José I. Espeso:** Methodology, Data curation. **Magdalena Lesniak:** Resources, Investigation. **Piotr Miluski:** Methodology, Investigation. **Sylvia Conzendorf:** Investigation. **Juliane Posseckardt:** Visualization, Methodology, Investigation, Data curation. **Zhongquan Liao:** Investigation. **Gloria Lesly Jimenez:** Resources, Methodology. **Martin Lorenz:** Methodology, Investigation. **Anka Schwuchow:** Methodology. **Martin Leich:** Writing – review & editing, Methodology, Investigation, Data curation. **Adrian Lorenz:** Investigation. **Katrin Wondraczek:** Writing – review & editing, Methodology. **Matthias Jäger:** Writing – review & editing, Writing – original draft, Methodology, Investigation, Funding acquisition, Formal analysis, Conceptualization.

Declaration of competing interest

The authors declare that they have no known competing financial interests or personal relationships that could have appeared to influence the work reported in this paper.

Acknowledgements

The project was funded by the European Union Horizon 2020 FET Open project NCLas—NanoCrystals in Fiber Lasers, No. 829161.

References

[1] B.N. Samson, P.A. Tick, N.F. Borrelli, Efficient neodymium-doped glass-ceramic fiber laser and amplifier, Opt. Lett. 26 (2001) 145–147. https://opg.optica.org/ol/abstract.cfm?URI=ol-26-3-145.

[2] G. Gorni, Jose J. Velázquez, M. Kochanowicz, D. Dorosz, R. Balda, J. Fernández, A. Durán, M.J. Pascual, Tunable upconversion emission in $NaLuF_4$–glass-ceramic fibers doped with Er^{3+} and Yb^{3+}, RSC Adv. 9 (2019) 31699–31707, https://doi.org/10.1039/C9RA05182A.

[3] J. Zhao, X. Zheng, E.P. Schartner, P. Ionescu, R. Zhang, T.L. Nguyen, D. Jin, H. Ebendorff-Heidepriem, Upconversion nanocrystal-doped glass: a new paradigm for photonic materials, Adv. Opt. Mater. 4 (2016) 1507–1517, https://doi.org/10.1002/adom.201600296.

[4] A. Lemiere, A. Szczodra, S. Vuori, B. Bondzior, T.W. Hawkins, J. Ballato, M. Lastusaari, J. Massera, L. Petit, Bioactive phosphate glass-based fiber with green persistent luminescence", Mater. Res. Bull. 153 (2022) 111899 https://doi.org/10.1016/j.materresbull.2022.111899.

[5] Z. Lu, N. Vakula, M. Ude, M. Cabi, T. Neisius, F. Orange, F. Pigeonneau, L. Petit, W. Blanc, $YbPO_4$ crystals in as-drawn silica-based optical fibers, Opt. Mater. 138 (2023) 113644, https://doi.org/10.1016/j.optmat.2023.113644.

[6] R. Müller, M. Lorenz, A. Veber, R. Sajzew, A. Kalide, J. Kobelke, A. Schwuchow, L. Kuusela, L. Wondraczek, L. Petit, K. Wondraczek, Fabrication and characterization of SiO_2 glass containing $YbPO_4$ crystals, Opt. Mater. Express 13 (8/1) (2023) 2322–2337, https://doi.org/10.1364/OME.495115.

[7] V. Fuertes, N. Grégoire, P. Labranche, S. Gagnon, N. Hamada, B. Bellanger, Y. Ledemi, S. LaRochelle, Y. Messaddeq, ACS Appl. Nano Mater. 6 (6) (2023) 4337–4348, https://doi.org/10.1021/acsanm.2c05449.

[8] P. Golonko, M. Kochanowicz, P. Miluski, D. Dorosz, A. Basa, J. Żmojda, Glass-ceramic optical fibers with controlled crystallization of core doped with europium ions, Ceram. Int. 50 (2024) 13652–13661, https://doi.org/10.1016/j.ceramint.2024.01.279.

[9] W. Blanc, B. Dussardier, Formation and applications of nanoparticles in silica optical fibers, J. Opt. 45 (3) (2016) 247–254, https://doi.org/10.1007/s12596-015-0281-6.

[10] T. Tran, A. Szczurek, A. Carlotto, S. Varas, G.C. Righini, M. Ferrari, J. Krzak, A. Lukowiak, A. Chiasera, Opt. Mater. 130 (2022) 112577, https://doi.org/10.1016/j.optmat.2022.112577.

[11] D. Dorosz, M. Kochanowicz, R. Valiente, A. Diego-Rucabado, F. Rodríguez, N. Siñeriz-Niembro, J.I. Espeso, M. Lesniak, P. Miluski, S. Conzendorf, J. Posseckardt, Z. Liao, G.L. Jimenez, R. Müller, M. Lorenz, A. Schwuchow, M. Leich, A. Lorenz, K. Wondraczek, M. Jäger, Pr^{3+}-doped YPO_4 nanocrystal embedded into an optical fiber, Sci. Rep. 14 (2024) 7404, https://doi.org/10.1038/s41598-024-57307-4.

[12] A. Veber, T. Salminen, A. Matthes, R. Mueller, K. Wondraczek, L. Petit, Synthesis, characterization, and optical properties of ytterbium(III) phosphates and their incorporation in different glass matrices, J. Phys. Chem. C 125 (2021) 702–715, https://doi.org/10.1021/acs.jpcc.0c07442.

[13] Ohara GmbH, S-NPH7 datasheet. https://www.ohara-gmbh.com/fileadmin/user_upload/export-data/pdf/product_datasheets/S-NPH7_English_.pdf. (Accessed 13 August 2024).

[14] Schott AG, Duran® datasheet, https://media.schott.com/api/public/content/e26004168cd944ad9026ce47d82f30a5?v=ed7dc95a, (accessed 13 August 2024).

[15] A. Einstein, On the movement of small particles suspended in a stationary liquid demanded by the molecular kinetic theory of heat, Ann. Phys. 17 (1906), 549 and 34 (1911) 591.

[16] R.E. Rosensweig, „Ferrohydrodynamics", Dover Publication, Inc., Mineola, N.Y., 1997 edition.

[17] T. Mattke, Rheologie-kurs. https://rheologie.hier-im-netz.de. (Accessed 9 September 2024).

[18] L. Boatner, Synthesis, structure, and properties of monazite, pretulite, and xenotime, Rev. Mineral. Geochem. 48 (1) (2002) 87–121.

[19] A. Kaminska, et al., Spectroscopy of f–f radiative transitions of Yb^{3+} ions in ytterbium doped orthophosphates at ambient and high hydrostatic pressures, J. Phys. Condens. Matter 22 (2010) 225902, https://doi.org/10.1088/0953-8984/22/22/225902.

[20] Jellison, et al., Spectroscopic refractive indices of metalorthophosphates with the zircon-type structure, Opt. Mater. 15 (2000) 103–109, https://doi.org/10.1016/S0925-3467(00)00027-6.